A Novel Classification of MRI Brain Images using ANFIS and 3D Reconstruction

M. Fathima Zahira, M. Mohamed Sathik

ABSTRACT--- The brain tumor (BT) has turn into a chief hazard to life in many humans. With the advances in medicine and technology, early tumor detection may pay a way for treating it in an early phase and thereby reducing the death rates. MRI imaging has a significant role in imaging the BT. Neurologist base the treatment of BT on the type, location, and also size of the tumor and hence proper segmentation of the tumor region has become essential. Here, an efficient segmentation algorithm is proposed, is centered on using the Sobel edge detection mechanism and the classification of the tumor region centered on the features extorted as of the segmented images are performed. The brain MRI images from a database which contain normal and also abnormal cases. These images are stripped from the skull by utilizing the morphological operations like morphological opening along with closing. Following this, segmentation is executed and finally, features are extorted as well presented to the classifier where the classification is executed. The segmentations algorithm is estimated and also the outcome are contrasted to the other prevailing algorithms say K-means and SVM (Support Vectors Machine) and the classification algorithm is weighted against that of the existent classification algorithm like PNN (probabilistic neural network) and ANN (Artificial Neural Network). Thus the proposed algorithms are confirmed to be superior to the other algorithms used in BT segmentations and classification.

Keywords: Sobel edge detection, Support Vector Machine, K-means algorithm, morphological operation, probabilistic neural network, Artificial Neural Network

I. INTRODUCTION

The formation of uncontrolled in addition to abnormal cells growth inside the skull is implied as a BT [1]. It is essentially of '2' types i) benign ii) malignant. Most terrible sorts of tumors are the malignant tumors [2]. Nevertheless, it would be unsuitable to identify benign as non-cancerous since it might be fatal too. The tumor could damage brain cells directly or indirectly squeezing disparate regions of the brain, as the tumor swells/grows within the brain causing rigorous pain. It is categorized by their position in the brain along with the tissue they are made of. Whether the tumor is benign or malignant, the reason behind tumor could well be hereditary or it could well be developed prior to birth like craniopharyngioma [3]. Tumors can well be detected utilizing procedures, like MRI (Magnetic Resonances imaging) in addition to CT (Computed Tomography). Usually, the MRI is extensively regarded initial imaging process on account of its multi-modality nature along with it is as well proficient in providing better information contrasted with CT. Manual BT segmentation on MRI images needs expert physicians. Furthermore, segmenting the entire voxels is an hard as well as a monotonous task [4]. Consequently, manual segmentation process typically defines coarse tumor delineations as well as gauges, to attain a coarse outline of the BT [5].

Numerous methods were posited and also developed for precise segmentation [6]. Segmentation of medicals images are difficult on account of poor image contrast together with artifacts which bring about missing/diffuse tissue boundaries [7]. A few of the top-notch techniques on the segmentation of the BT images take in K-mean clustering [8], SVM [9]. GA (Genetics Algorithm) is extensively utilized as an optimization algorithm; it is could be joined with the algorithms for instance SVM and ANN to attain better accuracy [10]. Some researchers have as well posited the utilization of morphological processes as well as edge detections algorithms say Sobel [11]. The segmented images are classified for identifying the normal and also the abnormal tumor regions centered upon the features obtained as of them. The performance of a range of classification algorithms explicitly SVM, K-Means, CART, KNN (K-nearest neighbours), Adaboost, chaos GA, EM technique, C4.5 was examined by the researchers centered upon classification accuracy along with kappa co-efficient. The outcomes illustrate that SVM encompass 97.15% as well as KNN encompass 96.94% accuracy. Consequently, KNN and also SVM give higher accuracy amid all algorithms [1]. Additionally, features could be extorted as of the segmentation images and they could be employed for training the deep learning algorithm such as CNN [12] in addition to the tumor could well be recognized with highest accuracy.

The remaining chapter is pre-arranged as: A concise discussion of the existing techniques associated to the work proposed is done in section2. In section3, the proposed technique is briefed. The outcomes of the proposed techniques are conferred in section4. Section 5 holds the conclusion.

II. LITERATURE SURVEY

Sérgio Pereira *et al.*[13] projected an automated segmentation process centered on CNN (Convolutionals Neural Networks), searching small 3×3 kernels. The usage of intensity normalizations as an initial pre-processing phase was as well investigated. This was authenticated in the BT Segmentation Challenge database (BRATS 2013), attaining concurrently the 1st position intended for the full, core, along with improving regions on Dices Similarity Coefficients metric (DSCM) of 0.830, 0.770, 0.880, aimed

Revised Manuscript Received on October 15, 2019

M. Fathima Zahira, Research Scholar, Bharathiar University, Coimbatore, Tamil Nadu, India.
(Email: fathimazahira.m@gmail.com)
Dr. M. Mohamed Sathik, Principal, Sadakathullah Appa College, Tirunelveli, Tamil Nadu, India.
(Email: mmdsadiq@gmail.com)

at the data set. Additionally, it attained the general 1st position through the online assessment platform. In the on-site BRATS 2015 Challenge utilizing the same design have participated, attaining the secondary place, with DSCM of 0.65, 0.78, and also 0.75 for the full, core, and also improving regions, correspondingly.

Kailash D. Kharat*et al*.[14] introduced the techniques that paid attention on the BT recognition utilizing feature extraction as well as selection from MRI Image. These methods combined the intensity and also the elements of the shapes along with the disparate order with the tumor textures as of the images. 3 sets of features explicitly, shape feature parameters, texture features parameters, and intensity feature parameter were extracted and also feature selection and reduction were performed utilizing PCA (Principal Components Analysis) and SGLDM (Spatial Gray Levels Dependence Matrices) respectively. Finally, they are graded using SVM.

N. Varuna Shree*et al.* [15] focused on noise removal method, extortion of gray-level co-occurrence matrix facets, DWT-centered BT region growing segmentation to lessen the intricacy as well as ameliorate the performance. Following this, the process of morphological filtering removed the noise that was formed subsequent to segmentation. The PNN was utilized for training and also for testing the performance accurateness in finding the tumor spot on MRI images. The investigational results attained almost 100 percent accuracy in recognizing normal as well as abnormal tissues as of brain MR images signifying the suggested technique's effectiveness.

Sudipta ROY*et al* [16] suggested a binarization which utilized standard deviation, mean, variance, and also entropy to ascertain a threshold value trailed in a non-gamut augmentation that could beat the binarization issue of brain element. A comparison was done amid the gotten outcome with this technique with regard to other renowned techniques. The comparisons verified that the recommended method aimed at image binarization outperforms other renowned methods. It overcame the issue of big intensity dissimilarity of foregrounds and backgrounds of MR images and it doesn't have any over binarizaion or under binarization issue for disparate sorts of images.

M.FathimaZahira*et al* [17] projected a technique for image segmentation together with 3-D image reconstruction. In the classification stage, the skulls Stripped images undergo segmentation through the watershed algorithm in an attempt to recognize the segmented tumor. After that, as of those segmented image, the traits like texture, shape, in addition to intensity were extorted. Then the traits were diminished through the PCA. Relying on the condensed traits, the PNN categorized the normal and also the abnormal (tumor) images. The subsequent stage is the 3D reconstruction; this planned the depth estimation for the image via the guided filters. And when the depth was gotten, the visual relics of the formed images' left and right view yielded the 3D reconstruction results.

III. PROPOSED METHODOLOGY

The proposed methodology's flow is portrayed in the below diagram

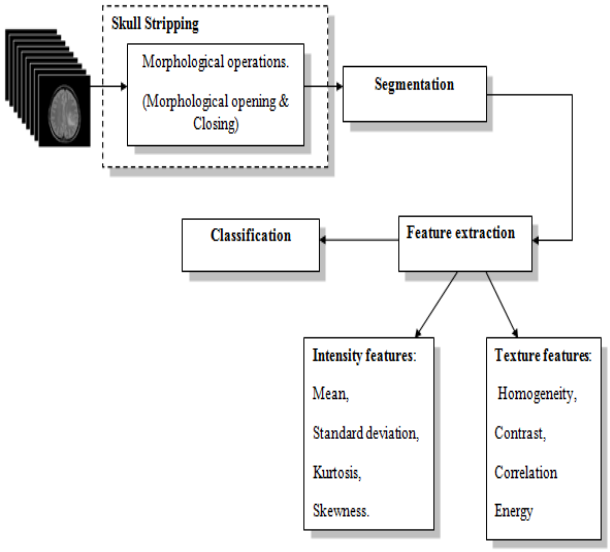

Figure 1 Flow of the proposed methodology

3.1. Skull Stripping

This is employed to segment the region of interest, that is, the brain is segmented as of the skull part in the MRI image. Let the input MRI image be signifiedas I_{mri}. This is performed by utilizing morphological processing and the resultant stripped image may be represented as S_{mri}. Initially, a disk-shaped structural element S_e is chosen, trailed by morphological Closing and opening of the inputted image is performed. In morphological the image is dilated and also then eroded. Step 1: Perform morphological closing, where dilation is trailed by erosion $A = I_p \bullet S_e = \left(f_p \oplus S_e\right) \Theta S_e$ (1)In (1) $\bullet$ represents dilation and $\circ$ represents erosion, I_p is the input image's pixel

Step 2: carry out morphological opening, where erosion is trailed by dilated

$$B = A_p \circ S_e = \left(A_p \Theta S_e\right) \oplus S_e \quad (2)$$

Where, A_p is the image's pixel after morphological closing

Step 3: The skull region is found as below,

$$J = I_{mri} - B \quad (3)$$

Step 4: Finally, the skulls stripped image is represent as *K* is obtained as,

$$K = I_{mri} - J \quad (4)$$

3.2. Segmentation

The proposed [segmentation] algorithm makes utilization of the sobel operation to spot the edges along with a threshold function. The sobel operator utilizes a 3×3 mask.

-1	-2	-1
0	0	0
1	2	1

(a) Sobel Mask

a_1	a_2	a_3
a_4	a_5	a_6
a_7	a_8	a_9

(b) 3×3 region

Figure 2 Mask of Sobel and the part of the image.

The gradients on the x as well as y axis may be signified as,

$$G_x = \frac{\partial k}{\partial x} = (a_7 + 2a_8 + a_9) - (a_1 + 2a_2 + a_3) \quad (5)$$

$$G_y = \frac{\partial k}{\partial y} = (a_3 + 2a_6 + a_9) - (a_1 + 2a_4 + a_7) \quad (6)$$

Thus the gradient of the images is defined as,

$$\Delta f(x,y) = \frac{\partial k}{\partial x}\hat{i} + \frac{\partial k}{\partial y}\hat{j} = G_x\hat{i} + G_y\hat{j} \quad (7)$$

Where, $\hat{i}$ *and* $\hat{j}$ are the unit vectors on a x as well as y axis likewise, the magnitudes of the gradient is provided by,

$$G(x,y) = |\nabla k(x,y)| = \sqrt{G_x^2 + G_y^2} \quad (8)$$

The next phase is to ascertain the threshold value, T_h the pixels with gradient greater than T_h are regarded as edge point and also is signified as a white pixel; if not it is selected as black. The edge-mapped image $T(x,y)$ therefore attained is:

$$T(x,y) = \begin{cases} 255 & G(x,y) \\ 0 & otherwise \end{cases} \quad (9)$$

After this, closed contours are found using the subsequent algorithm. The inputted images $T(x,y)$ are segmented by the proposed algorithm after thresholding into *r* segments and associate every pixel with the *r* regions. Let H_k denote the k^{th} region and initialize k with 0. Now the first pixel of a specific region H_r is known, after that to locate more pixels of this region, a search procedure is called. The algorithm is depicted below.

```
1. Begin
2.      for i= 1 to h
3.      for j=1 to w
4.              if T(x,y)=0
5.                      { for k=1 to r
6.                              if( T(x, y) ∈ region H_k )
7.                                      {goto step 1 to scan the next pixel
8.                                      }
9.                      r=r+1;
10.                     T(x, y) → H_r
11.                     call search
12.                     }
```

Figure 3 Closed Contour Algorithm Main

```
Search
13.     for n=1 to 8 pixel neighbors (T(x_0, y_o))
14.             {for k=1 to r
15.                     {if (T(x_n, y_n) ∈ region H_k)
16.                             {goto step 13 to scan the next neighbor
17.                             }
18.             for x=-2 to 2
19.                     for y=-2to2
20.                       if ((T(x_n + x, y_n + y) = 255) goto step 13
21.             T(x_n, y_n) → H_r
22.             call search
23.             }
24. End
```

Figure 4 Closed contour search algorithm

At the finish of this process, all the closed contours are detected. The very last step is to extract tumor as of this. The BT is extorted as of the region via detecting the utmost active regions of the brain.

$$T_u = H_{k|\mu_k} = \max\{\mu_1, \mu_2, \ldots\ldots \mu_r\} \quad (10)$$

Where H_k denotes the k^{th} region and as well μ_k signifies the average intensity of the pixels of MRI which overlaps with the region H_k

3.3. Feature extraction

As of the segmented image, the subsequent features are extorted.

Intensity features: Mean, Kurtosis, Standard deviation, and Skewness.

Texture features: Homogeneity, Contrast, Correlation, and Energy

These are then inputted to the ANFIS classifier for the categorization of the abnormal and the normal areas.

3.4. Classification.

The nodes on the 1st layer are adaptive; every node is defined through a membership function, which could be indicated as,

$$\mu_i(x) = \exp\left[-\left(\frac{x-m_i}{d_i}\right)^{2h_i}\right] \quad (11)$$

Where, d_i, h_i, m_i are the parameters to be learn

The nodes on the 2nd layer are signified by the function $\prod$ which denotes multiplication. The nodes on layer 2 synthesize the data from the former layers. The 2nd layer's output may be signified as w_j, $j = 1,2$. Later,the nodes are fixed.

$$w_1 = \mu_{Ci}(x_1).\mu_{D1}(x_2).\mu_{E1}(x_3).\mu_{F1}(x_4).\mu_{G1}(x_5).\mu_{H1}(x_6).\mu_{I1}(x_7).\mu_{J1}(x_8) \quad (12)$$

$$w_2 = \mu_{C2}(x_1).\mu_{D2}(x_2).\mu_{E2}(x_3).\mu_{F2}(x_4).\mu_{G2}(x_5).\mu_{H2}(x_6).\mu_{I2}(x_7).\mu_{J2}(x_8) \quad (13)$$

The nodes on 3rd layer are marked as N indicating the normalization of the firing strengths of the former layer. These are fixed and alsothereforesignified by circles. The 3rd layer's output may be signified as,

$$\bar{w}_1 = \frac{w_1}{w_1 + w_2} \quad (14)$$

$$\bar{w}_2 = \frac{w_2}{w_1 + w_2} \quad (15)$$

The 4th layer's outputmight be indicated as y, resulting as of the inferences of rules. The resulting output is just a result of normalized firing rule strength as well as 1st order polynomial. Weighted output of rule signified via node function as:

$$y_1 = \bar{w}_1 f_1 = \bar{w}_1(p_1x + q_1y + r_1) \quad (16)$$

$$y_2 = \bar{w}_2 f_2 = \bar{w}_2(p_2x + q_2y + r_2) \quad (17)$$

Parameters on this layer will be mentioned as resulting parameters. p_i, q_i, r_i are the linear parameters

Layer 5 is signified by the equations,

$$f = \sum_{1=1}^{2} \bar{w}i f_i = \frac{\sum_{i=1}^{2} w_i f_i}{w_1 + w_2} \quad (18)$$

The output of f is,

$$\left.\begin{aligned} f &= \frac{w_1}{w_1 + w_2} f_1 + \frac{w_2}{w_1 + w_2} f_2 \\ f &= \bar{w}_1(p_1x + q_1y + r_1) + \bar{w}_2(p_2x + q_2y + r_2) \\ f &= (\bar{w}_1 x)p_1 + (\bar{w}_1 y)q_1 + (\bar{w}_1)r_1 + (\bar{w}_2 x)p_2 + (\bar{w}_2 y)q_2 + (\bar{w}_2)r_2 \end{aligned}\right\} \quad (19)$$

The ANFIS structure is depicted below,

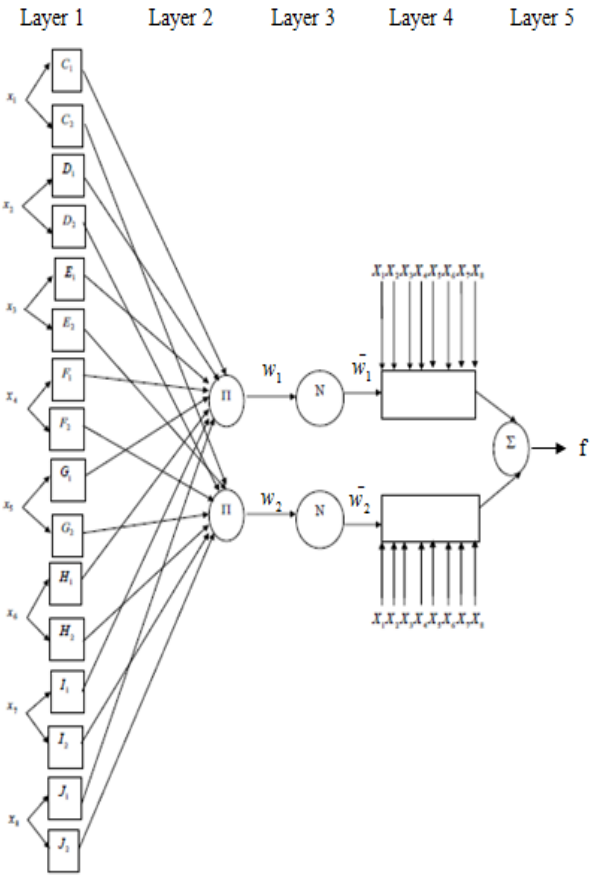

Figure 5 Structure of ANFIS classifier

3.5. 3D reconstruction.

MRI scans comprises a good deal of 2D slices that makes 3D reconstruction a intricate and tedious task. A proficient algorithm is posited aimed at 3D reconstruction with is described below.

Input:
Image I_{mri}

Begin
Linear co-efficient of the guided filter is calculated as,

$$E_k = \frac{\frac{1}{|\omega|}\sum I_{mri}(x,y)\hat{z}(x,y) - u_k \bar{m}_k}{\sigma_k^2 + \varepsilon} \quad (20)$$

$$E_k = \bar{m}_k - d_k u_k \quad (21)$$

The filter M(x,y) is constructed as,

$$M(x,y) = D_k \hat{z}(x,y) + E_k \quad (22)$$

Finally, depth map might be obtained as,

$$P(x,y) = \omega_3 * \left(\frac{1 - \hat{z}(x,y)}{Z_p}\right) \quad (23)$$

Step 1: Initially the linear coefficients of the filter, D_k, E_k is computed utilizing (20). In (20) $\hat{z}$ is the images of the guided filter, $|\omega|$ indicates the number of pixels and also $\bar{m}_k$ indicates the mean of the image.

Step 2: After the linear coefficients are attained the filter may be designed utilizing (21). The bilateral filters smoothens the image whilst maintaining the edges, hence the redundant information gets eliminated.

Step 3: at the present, since the depth map is attained the parallax for every pixel (x,y) may be computed utilizing (22). In (22) z_p is the zero parallel plane. And ω_3 stands as a constant value and fixed to be 0.5.

Step 4: to generate the left together right view of the image each pixel is moved $(x, y)/2$ to the left or the right direction.

IV. RESULTS AND DISCUSSION

4.1. Performance analysis

The proposed work's performance is assessed concerning the statistical parameters like specificity, sensitivity, accuracy, FPR (false positives Rate), together with FNR (false negatives rate). And the results are contrasted to the prevailing techniques. Also, the efficiency of classification betwixt normal and abnormal tissues is evaluated concerning FRR (False Rejections Rate), FAR (False acceptances Rate), MCC (Mathews Correlations Coefficient), these are also compared with the exiting techniques.

4.1.1. Analysis of segmentation techniques.

4.1.1.1. Dice Similarity Coefficient

It is basically a statistic utilized aimed at similarity comparison of 2 samples.

$$DSC = \frac{2T_p}{2T_p + F_p + F_n} \tag{24}$$

Where, T_n is true negative, and F_p is false positive

4.1.1.2. Sensitivity

The sensitivity is computed utilizing the below formula,

$$Sensitivity = \frac{T_p}{T_p + F_n} \tag{25}$$

Where, T_p is true positive, F_n is false negative,

4.1.1.3. Specificity

It stands as the percentages of the true negatives properly recognized by an analytical test. It reveals how efficiently the test identifies the normal (i.e., negative) circumstance.

$$Specificity = \frac{T_n}{F_p + T_n} \tag{26}$$

4.1.1.4. False positive Rate

This is at the rate wherein the normal tissues are mis-classifieds as abnormal tissues.

$$FPR = \frac{F_p}{F_p + T_n} \tag{27}$$

4.1.1.5. False negative rate

This is the rate at which the abnormal tissues are mis-classified as normal tissues.

$$FNR = 1 - \left(\frac{T_p}{T_p + F_p} \right) \tag{28}$$

The above stated performance measures are graphical represented in the below figure

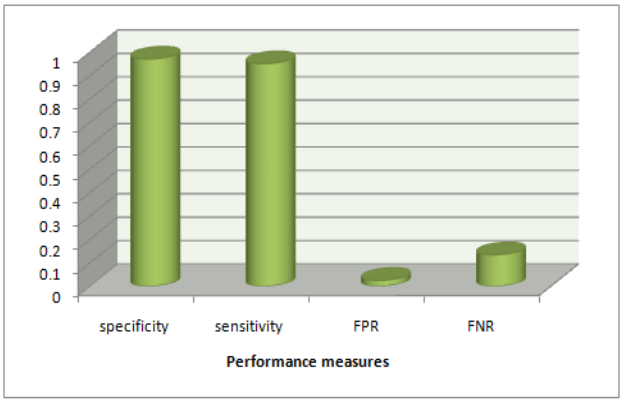

Figure6 Performance measures of the proposed segmentation technique.

The fig.6offersvisual evidence aimed at the proposed algorithm's efficiency. It is obvious that the proposed work has a high right classification rate and also a low mis-classification rate, therefore making it an efficient algorithm.

4.1.2. Analysis of classification techniques.

4.1.2.1. F1 Score.

F1 Score indicates the Harmonics Mean betwixt recall and precision. The range for F1 Score is [0, 1]. It tells how precise your classifier is (i.e., how numerous instances it classifies properly), in addition how robust it is (i.e., it doesn't miss a major number of instances).The bigger the F1 Score, the superior is the proposed model's performance

$$F_1 = 2 \times \left(\frac{1}{\frac{1}{p_r} + \frac{1}{R_e}} \right) \tag{29}$$

Where P_e is the precision, it stands as the number of corrects positive outcome divided with the numbers of positive outcome forecasted by the classifier, it is given by,

$$P_e = \frac{T_p}{T_p + F_p} \tag{30}$$

R_e is the recall, It stands as the numbers of correct positive outcome divided with the numbers of ***all*** pertinent samples (all samples that ought to have been recognized as positive), it is signified by,

$$R_e = \frac{T_p}{T_p + F_n} \quad (31)$$

4.1.2.2. Accuracy.

$$A_c = \frac{T_n + T_p}{T_n + T_p + F_n + F_p} \quad (32)$$

The Recall, accuracy in addition to Precision of the proposed system is represented graphically below,

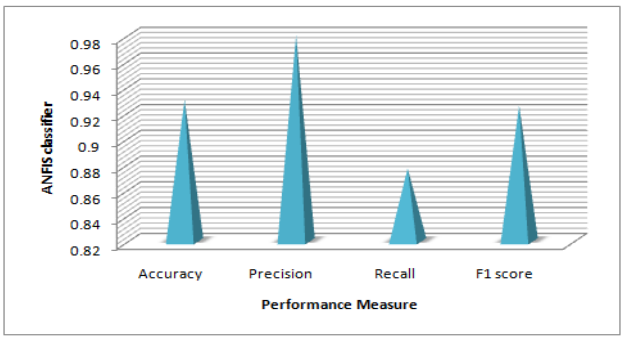

Figure7Performance measures of ANFIS

4.2. Comparative Analysis.

4.2.1. Segmentation Algorithm.

The proposed technique's performance is assessed by contrasting to the prevailing works; here comparison is done with the existing techniques like SVM and k-means algorithm. Figure portrays the comparison of the dice coefficient. It is computed utilizing (24).

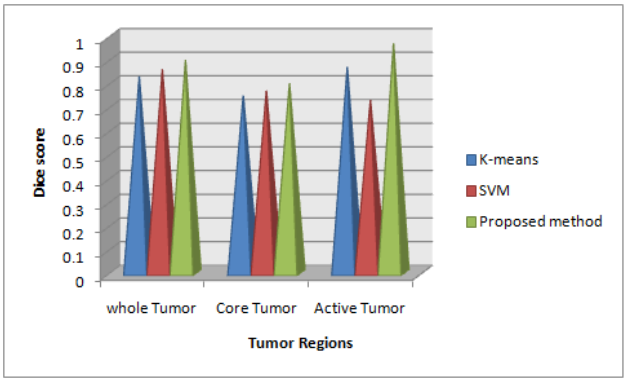

Figure8 Dice score comparison

The above figure provides a Dice coefficients' comparison. The higher is the dices coefficient value; the better is the segmentations process. Form the figure it is evident that the proposed work shows higher dice coefficient values contrasted to the other top-notch techniques taken for comparison, thus proving it to be an efficient segmentation techniques for MRI images.

The other performance metrics discussed above are also compared. The sensitivity stands as the TPR (true positives rate), that is, the rate at which the segmentations algorithm correctly segments the tumor region. The sensitivity is calculated using (25). Specificity is the TPR, that is, the rate at which the segmentations algorithm correctly segments the non-tumor region as normal. This is calculated using (26).

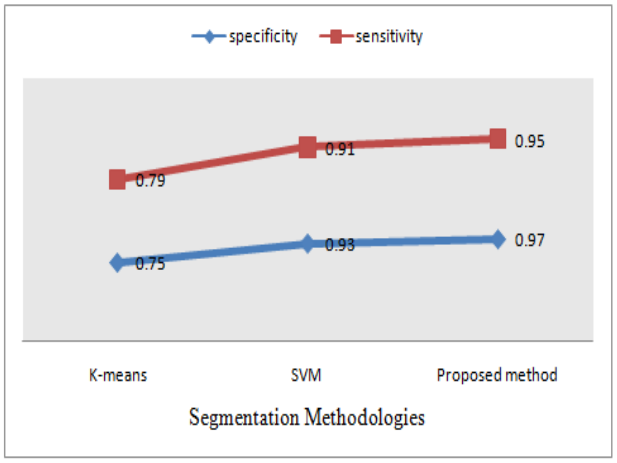

Figure9Sensitivity and specificity comparison

The above figure gives adelineation of the variations on specificity and also sensitivity of the segmentations algorithms. As evident as of the figure 10, the proposed one beats the existing methods.

The segmentation algorithms can well be also compared concerning their misclassification. The algorithm lower mis-classification rate is considered to be an efficient one. The misclassifications can well be estimated as of the FPR and also the FNR. These are computed utilizing (27) and (28).

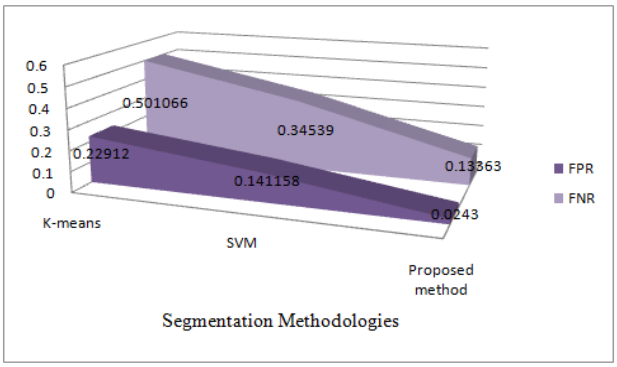

Figure 10FPR and FNR comparison.

The above figure gives an efficient comparison of FNR and FPR of the proposed and the existing segmentation methodologies. From the figure, it is obvious that when contrasted with the prevailing segmentation algorithm, the proposed one is better.

The results discussed above are linked in the table 1.

Table 1 Performance measure of segmentation Algorithm

Methodologies	Specificity	Sensitivity	FPR	FNR
K means	0.75	0.79	0.22912	0.501066
SVM	0.93	0.91	0.141158	0.34539
Proposed segmentation	0.97	0.95	0.0243	0.13363

4.2.2. Classification Algorithms.

The proposed ANFIS classifier's efficiency is proved by this comparison analysis. Here ANFIS is contrasted to the prevailing classification algorithms such as PNN and ANN. Initially the F1 Score is compared. The comparison is

exhibited in the fig 11. This gives a clear interpretation of the F1 Score of the posited ANFIS algorithm and how they vary relying on the effectiveness of the disparate classification techniques.

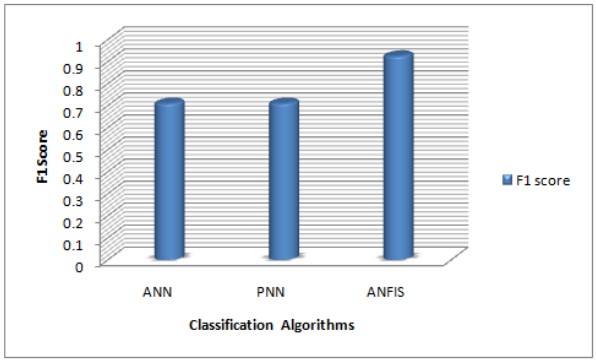

Figure11F1 Score comparison.

From the figure, it is apparent that the F1 score of ANFIS is higher comparing the existing techniques. Thus it proves that ANFIS is a superior classifier.

The classification technique's performance can be also evaluated on the base of its precision, accuracy, and also recall values. In the following figure comparison of these performance measures are made.

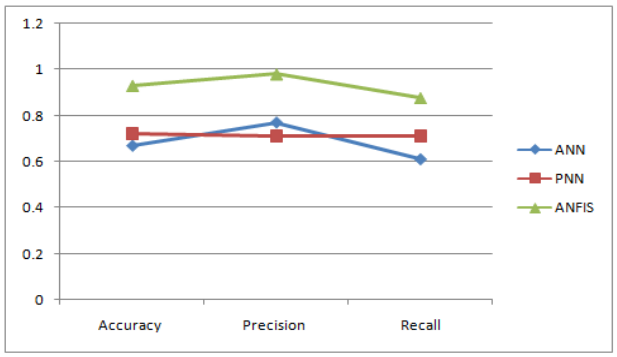

Figure12Comparisons of Accuracy, Precision and Recall.

The above figure provides a strong evidence for the efficiency of the classification algorithm proposed. Thus from the above comparisons made on the base of the F1 Score, accuracy, precision, together with recall, can conclude that ANFIS is superior to the top-notch segmentation techniques.

The Performance measures of the Classification techniques are concatenated in the 2nd table.

Table 2 Performance measures of the classification Algorithm.

Methods	Accuracy	Precision	Recall	F1 score
ANN	0.67	0.77	0.611897	0.710532
PNN	0.722	0.71	0.711065	0.710532
ANFIS	0.93	0.98	0.876683	0.925467

V. CONCLUSION

An effective segmentation as well as classification methodology is proposed here. The segmentations algorithm is evaluated concerning the DSC, sensitivity, specificity, FNR and FPR and was assessed concerning Recall, Accuracy, Precision, and also F1 score. Form the performance analysis, a clear notion about the proposed algorithms' efficiency can be understood. An algorithm aimed at 3-D reconstruction of the image is also proposed here. This provides an effective 3-D model of the MRI brain images.

REFERENCES

1 Chauhan, Saumya, Aayushi More, Ritumbhra Uikey, Pooja Malviya, and Asmita Moghe. "Brain tumor detection and classification in MRI images using image and data mining." In *Recent Innovations in Signal processing and Embedded Systems (RISE), 2017 International Conference on*, pp. 223-231. IEEE, 2017.

2 Amin, Javeria, Muhammad Sharif, Mussarat Yasmin, and Steven Lawrence Fernandes. "Big data analysis for brain tumor detection: Deep convolutional neural networks." *Future Generation Computer Systems* (2018).

3 Hazra, Animesh, Ankit Dey, Sujit Kumar Gupta, and Md Abid Ansari. "Brain tumor detection based on segmentation using MATLAB." In *2017 International Conference on Energy, Communication, Data Analytics and Soft Computing (ICECDS)*, pp. 425-430. IEEE, 2017.

4 Cabria, Ivan, and Iker Gondra. "MRI segmentation fusion for brain tumor detection." *Information Fusion*, Vol. 36, pp. 1-9, 2017.

5 Pinto, Adriano, Sérgio Pereira, Deolinda Rasteiro, and Carlos A. Silva. "Hierarchical Brain Tumour Segmentation using Extremely Randomized Trees." *Pattern Recognition*(2018).

6 Abdulraqeb, A. R. A., W. A. Al-haidri, and L. T. Sushkova. "A novel segmentation algorithm for MRI brain tumor images." In *2018 Ural Symposium on Biomedical Engineering, Radioelectronics and Information Technology (USBEREIT)*, pp. 1-4. IEEE, 2018

7 Chandra, G. Rajesh, and Kolasani Ramchand H. Rao. "Tumor detection in brain using genetic algorithm." *Procedia Computer Science* Vol. 79, pp. 449-457, 2016

8 Kaur, Navpreet, and Manvinder Sharma. "Brain tumor detection using self-adaptive K-means clustering." In *2017 International Conference on Energy, Communication, Data Analytics and Soft Computing (ICECDS)*, pp. 1861-1865. IEEE, 2017.

9 Shankaragowda, B. B., M. Siddappa, and M. Suresha. "A novel approach for the brain tumor detection and classification using support vector machine." In *2017 3rd International Conference on Applied and Theoretical Computing and Communication Technology (iCATccT)*, pp. 90-93. IEEE, 2017.

10 Chithambaram, T., and K. Perumal. "Brain tumor segmentation using genetic algorithm and ANN techniques." In *2017 IEEE International Conference on Power, Control, Signals and Instrumentation Engineering (ICPCSI)*, pp. 970-982. IEEE, 2017.

11 Aslam, Asra, Ekram Khan, and MM Sufyan Beg. "Improved edge detection algorithm for brain tumor segmentation." *Procedia Computer Science, Vol.* 58, pp. 430-437, 2015.

12 Parihar, Anil Singh. "A study on brain tumor segmentation using convolution neural network." In *Inventive Computing and Informatics (ICICI), International Conference on*, pp. 198-201. IEEE, 2017.

13 Pereira, Sérgio, Adriano Pinto, Victor Alves, and Carlos A. Silva. "Brain tumor segmentation using convolutional neural networks in MRI images." *IEEE transactions on medical imaging* Vol.35, no. 5, pp.1240-1251, 2016

14 Kharat, Kailash D., Vikul J. Pawar, and Suraj R. Pardeshi. "Feature extraction and selection from MRI images for the brain tumor classification." In *Communication and Electronics Systems (ICCES), International Conference on*, pp. 1-5. IEEE, 2016.

15 Shree, N. Varuna, and T. N. R. Kumar. "Identification and classification of brain tumor MRI images with feature extraction using DWT and probabilistic neural network." *Brain informatics*, Vol.5, no. 1, pp. 23-30, 2108

16 Roy, Sudipta, Debnath Bhattacharyya, Samir Kumar Bandyopadhyay, and Tai-Hoon Kim. "An improved brain MR image binarization method as a preprocessing for abnormality detection and features extraction." *Frontiers of Computer Science*, Vol. 11, no. 4, pp. 717-727, 2017.

17 Zahira, M. Fathima, and M. Mohamed Sathik. "An Efficient Classification of MRI Brain Images and 3D Reconstruction Using Depth Map Estimation." *Advances in Computational Sciences and Technology*, Vol.10, no. 5, pp. 1057-1080, 2017.